

Interaction of streamers and stationary corrugated ionization waves in semiconductors

A. S. Kyuregyan*

All-Russia Electrical Engineering Institute, 12 Krasnokazarmennaya St., 111250 Moscow, Russian Federation

(Received 19 December 2013; published 28 April 2014)

A numerical simulation of evolution of an identical interacting streamers array in semiconductors has been performed using the diffusion-drift approximation and taking into account the impact and tunnel ionization. It has been assumed that the external electric field E_0 is static and uniform, the background electrons and holes are absent, the initial avalanches start simultaneously from the nodes of the plane hexagonal lattice, which is perpendicular to the external field, but the avalanches and streamers are axially symmetric within a cylinder of radius R . It has been shown that under certain conditions, the interaction between the streamers leads finally either to the formation of two types of stationary ionization waves with corrugated front or to a stationary plane ionization wave. A diagram of different steady states of this type of waves in the plane of parameter E_0, R has been presented, and a qualitative explanation of the plane partition into four different regions has been given. Characteristics of corrugated waves have been studied in detail and discussed in the region of R and E_0 large values, in which the maximum field strength at the front is large enough for the tunnel ionization implementation. It has been shown that corrugated waves ionize semiconductors more efficiently than flat ones, especially in relatively weak external fields.

DOI: [10.1103/PhysRevE.89.042916](https://doi.org/10.1103/PhysRevE.89.042916)

PACS number(s): 89.75.Kd, 51.50.+v, 52.35.-g, 52.80.-s

I. INTRODUCTION

The streamer mechanism of electric discharge has been used for a long time for the description of pulse breakdown of various matters. A set of works is devoted to theoretical and experimental study of streamers; however, between these two ways of research there is an essential discrepancy. In vast majority of the theoretical works performed by both analytical and numerical methods, single streamers were studied. Meanwhile in practice the discharge is usually carried out by a large number of interacting streamers. Such electrostatic interaction has to be essential, in particular, in a pulse crown and in a streamer zone of a long spark where the characteristic distance between streamers is less than their lengths, but there is more than their diameters [1,2]. Excellent photos that especially visually illustrate this circumstance have been made in the last years (see, for example, Refs. [3,4]). Modeling of such multistreamer discharges is a very complex three-dimensional problem, so as a first step towards its solution a very simplified situation should be studied: the evolution of an identical streamers, which simultaneously starts from nodes of a one-dimensional (in this case, the model corresponds to experiments [5,6]) or two-dimensional periodic lattice.

As far as we know, the first attempt of this kind was made in Ref. [7] whose author studied evolution of the one-dimensional periodic array of the cylindrical streamers propagating in air from a thin wire to the plane parallel to it. Interaction between the charged streamers was taken into account by the approximate analytical solution of the corresponding electrostatic problem and introduction of thus obtained amendments to the field strength in a numerical model of a single streamer. It was shown that field strength before the front of each streamer in the array and the speed of their propagation considerably decrease in comparison with a single streamer. This result is quite expected. However, the author [7]

did not manage to receive any additional information, because in the framework of the so-called 1.5-dimensional numerical model which he used, the cross sizes and a form of each streamer are a priori set and therefore are not subject to interstreamer interaction.

This shortcoming is absent in Ref. [8], whose authors simulated the evolution of a two-dimensional periodic array of negative streamers in gases in a uniform external field E_0 , using a “minimal model” (taking into account the drift, diffusion, and impact ionization of electrons, background electrons are absent, and additional mechanisms of ionization are not taken into account [9]). At the initial stage, streamers develop independently from each other so that their length and front curvature radius increase with constant velocities [10,11]. But the nature of further evolution depends strongly on the distance $2L$ between streamers. If L is greater than some critical value $L_c(E_0)$, the front of each streamer starts quickly becoming distorted as a result of transverse instability, described in Refs. [12–16] for gases and in Refs. [11,17] for semiconductors. However, at $L < L_c(E_0)$ this instability is suppressed, and eventually the propagation of the streamers array becomes stable and self-similar: all of them travel with constant velocity u_f and an unaltered form of the front, which does not depend on the initial conditions and can be described by a multivalued function

$$y_f(x) = \frac{2}{\pi} bL \arccos \left[\exp \left(\frac{\pi x - x_f}{2 aL} \right) \right], \quad (1)$$

where $x_f = u_f t$ is a front position on the axis x parallel to the external field, y_f is a distance from the axis x to the front, $b < 1$, and a are adjustable parameters. This formula was obtained in Ref. [18] to describe the shape of the interface between two incompressible fluids with very different viscosities (for example, water, which forces the glycerin) moving in the narrow gap between two plates with width $2L$ (Hele-Shaw cell) [19,20]. In this case the boundary velocity u_f is $(1 + a/b)$ times more than velocity u_0 of a viscous fluid

*ask@vei.ru

far ahead the border, and therefore the matter conservation law provides the relation

$$a + b = 1. \quad (2)$$

The formula (1) is also applicable to describe a number of other physically different but mathematically equivalent processes, provided that the normal velocity of the interface u_n at each point is proportional to the gradient of some potential function $\varphi(x, y)$, which satisfies the Laplace equation, and the interface itself is equipotential:

$$\varphi(x, y_f) = \text{const}, \quad u_n \propto E_n \equiv |\nabla_n \varphi(x, y_f)|. \quad (3)$$

In experiments with Hele-Shaw cells (in this case, φ is pressure) it always gets $b = 1/2$, that is, after the establishment of the steady state motion of the interface less viscous liquid supplants exactly half of the cell width. This nontrivial selection phenomenon was explained by the influence of a small, but finite deviation from the first condition in (3) because of the surface tension [19,20] or kinetic undercooling [21].

A model of streamers satisfying conditions (3) (in this case, φ is electric potential) was first used in Ref. [22] (see also the book [23]) and was improved later in Refs. [10,24], but in fact they can be performed only very approximately. Violation of the former is due to the finite conductivity of the plasma behind the front and nonzero thickness δ of the front, and the latter to a more complicated dependence of u_n on the field strength E_n normal to front. Within the framework of the “minimal model” of streamers in gases, with some reservations, it is possible to use the formula [9,25]

$$u_n = u^* \equiv v_e + 2D_e \lambda^*, \quad (4)$$

where $\lambda^* = \sqrt{v_e \alpha_e / D_e}$ is a parameter of exponential decay of the electron concentration n ahead of the front, and v_e , D_e , and α_e are a drift velocity, a diffusion coefficient, and an impact ionization coefficient, which locally depend on E_n . Usually in gases the second term in the right-hand side of (4) is relatively small [9,25], so at a constant electron mobility μ_e front velocity $u_n \approx \mu_e E_n$. This is a fact the authors of Ref. [8] deemed a sufficient basis for applicability of formula (1) to interpret their results of numerical simulations, in particular, the approximate ratio¹ $E_M \equiv E_n(x_f, 0) = 2E_0$; however it was ignored that in the case of streamers there was no reason for equality (2).

The study of a similar problem with regard to semiconductors is also very important. In practical terms, this is due to the fact that multistreamer breakdown mechanism determines (at least in some regimes) [26,27] the operation of avalanche voltage sharpeners, which are commutators with unique characteristics [28,29], but in scientific terms this is due to features of microscopic processes in semiconductors. Among them there are particularly important ones:

(1) Saturation of dependencies $v_{e,h}(E)$ in relatively very low fields $E \sim E_s \sim 10$ kV/cm, which, in particular, leads to significantly (relative to gas) increasing the ratio $u_n/v_{e,h}$

even within the framework of the “minimal model” of streamers [30,31] and

(2) Existence of tunneling ionization, which can also increase the ratio of $u_n/v_{e,h}$ by orders of magnitude [11,32–37].

These features lead to the fact that $u_n \propto E_n$ only at $E_n \ll E_s$, but in the usual range of $E_n \sim 10\text{--}10^3$ kV/cm function $u_n(E_n)$ varies from constant to exponentially strong. Therefore, the second of the conditions (3) is never executed, and Eq. (2) can be satisfied only by chance at some relations between the parameters of the problem. Such a radical change in the classical formulation of the problem [19,20] can lead to substantially different scenarios of evolution of the interface between the phases in a highly nonequilibrium conditions.

In this paper, we study this interesting problem by numerical simulation of the interaction between the streamers in semiconductors. The main aim of this work is to obtain maximally detailed and complete results for the simplest case of a static uniform external field E_0 , which can provide the basis for further research.

II. MATHEMATICAL MODEL OF STREAMERS ARRAY

Similar to the most works on the numerical simulation of streamers, the diffusion-drift approximation is used. In this approximation, the distributions of electrons, $n(t, \mathbf{r})$, and holes, $p(t, \mathbf{r})$, are described by the continuity equations, which we conveniently write in the form

$$\frac{\partial(p+n)}{\partial t} + \nabla \cdot (\mathbf{j}_h + \mathbf{j}_e) = 2(s_g - s_r), \quad (5)$$

$$\frac{\partial(p-n)}{\partial t} + \nabla \cdot (\mathbf{j}_h - \mathbf{j}_e) = 0, \quad (6)$$

where the terms $s_{g,r}$ describe all possible mechanisms of generation and recombination, and the free carrier flux densities are given by the expression

$$\mathbf{j}_e = v_e n - \nabla(D_e n), \quad \mathbf{j}_h = v_h p - \nabla(D_h p),$$

where the subscripts e and h correspond to electrons and holes, respectively. In this paper, we considered only indirect-gap semiconductors such as Si, Ge, or SiC, in which the rate of radiative recombination (and, hence, photoionization rate) is very small. Therefore the generation of pairs occurs primarily due to the impact and tunnel ionization; consequently, the generation rate has the form

$$s_g = (\alpha_e v_e n + \alpha_h v_h p) h(n + p - n_{th}) + g_t,$$

where $h(x)$ is the Heaviside unit step function, and n_{th} is a certain threshold density. It is introduced in order to exclude the appearance of nonphysical solutions due to the impact ionization far ahead of the streamer front, where the densities of the electrons and holes generated by the tunnel ionization in the external field are very low ($n + p < n_{th}$) and the continual approximation is certainly inapplicable [32,38]. Under the assumption that the lifetime of charge carriers is much larger than the propagation time of the streamers, recombination is disregarded; i.e., $s_r = 0$ is set. Moreover, the impact ionization coefficient $\alpha_{e,h}$, drift velocities $v_{e,h}$, and tunnel ionization rate g_t are assumed to be specified instantaneous and local

¹This ratio is rather well performed for the streamers array investigated in Ref. [8] at the highest values of $L < L_c$, when $\delta \ll L$ and the deviation from the first condition (3) is minimal.

functions of the field strength $\mathbf{E}(t, \mathbf{r})$, satisfying the Poisson equation

$$\nabla \cdot \mathbf{E} = \frac{q}{\varepsilon}(p - n) = -\Delta\varphi, \quad (7)$$

where φ is the electric potential, q is the elementary charge, and ε is the permittivity of the semiconductor. The usual approximations,

$$\begin{aligned} \mathbf{v}_h &= -\mathbf{v}_e = \mu \mathbf{E}, \quad \mu = v_s/(E + E_s), \\ \alpha_e &= \alpha_h = \tilde{\alpha} \exp(-\tilde{E}/E), \\ g_t &= \tilde{g}_t (E/E_t)^2 \exp(-E_t/E), \end{aligned}$$

are used, and the dependence of the diffusion coefficients $D_{e,h}$ on E is disregarded, i.e., $D_e = D_h = D = \text{const}$. The parameters v_s , E_s , $\tilde{\alpha}$, \tilde{E} , \tilde{g} , and E_t are determined by the band structure of semiconductors and electron and hole scattering mechanisms. We used the same typical values $v_s = 10^7 \text{ cm/c}$, $E_s = 15 \text{ kV/cm}$, $\tilde{\alpha} = 10^6 \text{ cm}^{-1}$, $\tilde{E} = 1.5 \text{ MV/cm}$, $\tilde{g} = 6.7 \times 10^{35} \text{ cm}^{-3} \text{ s}^{-1}$, $E_t = 22.5 \text{ MV/cm}$, $D = 20 \text{ cm}^2 \text{ c}^{-1}$, and $\varepsilon = 11.8\varepsilon_0$, as in Ref. [11].

The initial conditions for the system of equations (5)–(7) have the form

$$\varphi(0, \mathbf{r}) = -E_0 x, \quad (8)$$

$$\sigma(0, \mathbf{r}) = \sigma_0(\mathbf{r} - \mathbf{r}_i), \quad \rho(0, \mathbf{r}) = 0, \quad (9)$$

where E_0 is the strength of the external field, which is directed along the x axis, $\sigma = q(p + n)/\varepsilon\tilde{\alpha}\tilde{E}$ and $\rho = q(p - n)/\varepsilon\tilde{\alpha}\tilde{E}$ are dimensionless concentration and the space charge density of electrons and holes, and $\sigma_0(\mathbf{r})$ is any quite strongly localized function satisfying the normalization condition $\int \sigma_0(\mathbf{r}) d\mathbf{r} = 2q/\varepsilon\tilde{\alpha}\tilde{E}$. The Gaussian distribution is used,

$$\sigma_0(\mathbf{r}) = \sigma_0^0 \exp(-r^2/r_\sigma^2), \quad (10)$$

where $\sigma_0^0 = 2q/\pi^{3/2}\varepsilon\tilde{\alpha}\tilde{E}r_\sigma^3$. These initial conditions correspond to the appearance of one electron hole pair at each point $\mathbf{r} = \mathbf{r}_i$ at time $t = 0$. In accordance with what was said in the introduction, these points coincide with the nodes of a planar, for example, hexagonal, lattice located in the plane $x = 0$. In this case, avalanches and streamers generated by them have the symmetry of a regular hexagonal prism. Therefore, in the cylindrical coordinate system $\mathbf{r} = \{x, y, \vartheta\}$ (hereinafter y is the distance from the point \mathbf{r} to axis x , and ϑ is the azimuthal angle), strictly speaking, one should take into account the dependence of n, p , and φ on ϑ , which is necessary to solve the three-dimensional Cauchy problem with natural boundary conditions on the lateral faces of the prism, which requires very large computing resources. Meanwhile, the problem can be considerably simplified if a prism with the width of the lateral faces H is approximate by a cylinder with a radius $R = H\sqrt{3}\sqrt{3}/2\pi \approx 0.91H$. In this case the area of the base of a prism and cylinder are the same, and the distance between their lateral surfaces does not exceed $0.1H$. Such a small difference between forms of the side surfaces should not have a significant impact on the processes of ionization and transport near the axis of symmetry, which mainly determines the evolution of an array of streamers. To confirm the validity of this statement the main parameters (the maximum field

strength on the front E_M , the concentration of electrons and holes in the x axis behind the front σ^- , and the front velocity u_f) of a plane, axially and hexagonal symmetrical streamers obtained by modeling with the same finite element meshes are shown in the table below. As can be seen, the parameters of the plane streamer differ significantly from almost matching parameters of axially and hexagonal symmetrical streamers. At the same time, the dimensionless computing speed $\Delta x_f/\Delta t v_s$ (here Δt is the time spent modeling the process of promoting the front on the distance Δx_f) for a hexagonal streamers almost 100 times less than for an axially symmetric one. Therefore, in this paper we neglect the dependencies of $n, p, \varphi(\vartheta)$, weak at actual values of $y \lesssim H/2 \approx R/2$, and assume that avalanches and streamers have axial symmetry.

Parameters of various streamers at
 $E_0 = 0.5\tilde{E}$, $L = R = 0.91H$, $H = 289/\tilde{\alpha}$

Parameter	Plane	Axial	Hexagonal
E_M/\tilde{E}	0.773	1.17	1.18
σ^-	0.17	0.58	0.59
u_f/v_s	1.88	4.14	4.12
$\Delta x_f/\Delta t v_s$	0.36	0.15	0.0017

Under the above assumptions, our task is also symmetrical with respect to the plane $x = 0$, so it is enough to solve it in a rectangular area,

$$0 \leq x \leq X, \quad 0 \leq y \leq R, \quad (11)$$

the length of which X should be much longer than streamer length. In this case, the boundary conditions take the form

$$\begin{aligned} \varphi(t, 0, y) = 0, \quad \partial\varphi(t, x, y)/\partial x|_{x=X} = E_0, \\ \partial\varphi(t, x, y)/\partial y|_{y=0, R} = 0, \end{aligned} \quad (12)$$

$$\sigma(t, X, y) = 0, \quad (13)$$

$$\partial\sigma(t, x, y)/\partial x|_{x=0} = \partial\sigma(t, x, y)/\partial y|_{y=0, R} = 0,$$

$$\rho(t, X, y) = \rho(t, 0, y) = 0 \quad (14)$$

$$\partial\rho(t, x, y)/\partial y|_{y=0, R} = 0.$$

The Cauchy problem (5)–(14) was solved by the finite element method with adaptive nonuniform mesh in the way described in Ref. [11].

III. RESULTS AND DISCUSSION

The calculations were performed for values $E_0 = (0.2-0.7)\tilde{E}$ and $R = (20-8000)\tilde{\alpha}^{-1}$. The simulation results are presented in Figs. 1–13. They are very weakly dependent on the choice of the quantities r_σ [36] and $\sigma_{th} = qn_{th}/\varepsilon\tilde{\alpha}\tilde{E}$ [11]; in the present study, we used the values $r_\sigma = 2/\tilde{\alpha}$ and $\sigma_{th} = 10^{-8}$.

As might be expected, avalanches and streamers develop independently from each other as described in Ref. [11], while their length $2x_f \ll 2R$. At $x_f = (2.5-3)R$ an electrostatic interaction between them becomes significant (see the

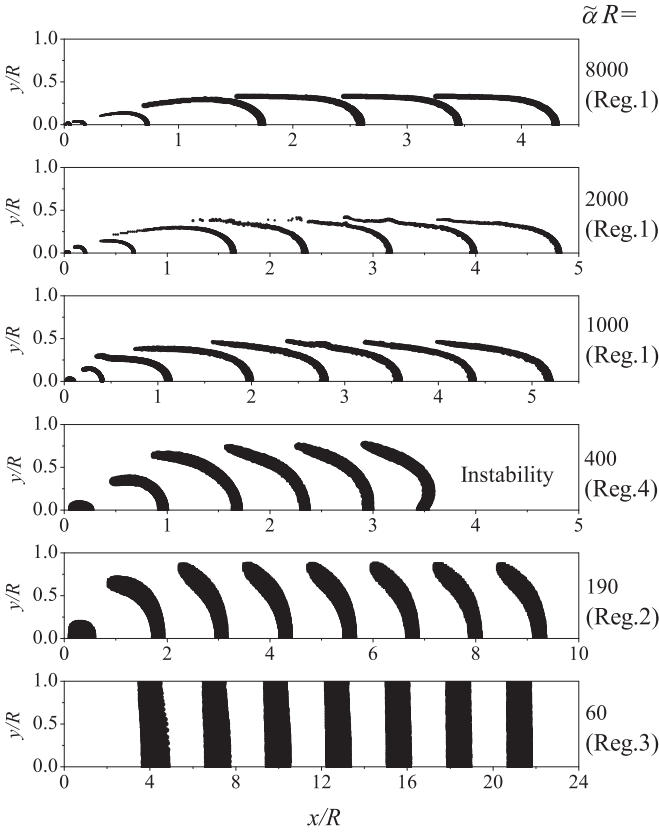


FIG. 1. The evolution of fronts of identical streamers, which starts simultaneously from a planar hexagonal lattice nodes, with $E_0 = 0.36\tilde{E}$ and different R . The relevant areas of the plane $[1/E_0, R]$ (see Fig. 3) are indicated in parentheses. Black indicates the zone of the front, inside which the space charge density is greater than $0.002\varepsilon\tilde{\alpha}\tilde{E} \approx 3,2 \text{ mC/m}^3$ at times $t = i/\tilde{\alpha}v_s \approx 10i \text{ ps}$, $i = 1, 2, \dots, 8$.

Appendix). At first, it slows down the expansion of streamers (Fig. 1) and reduces the maximum field strength E_M at the front (Fig. 2). Further results of the interaction depend strongly on the values of the control parameters E_0 and R . It turns out that the plane of $[1/E_0, R]$ splits into four regions shown in Fig. 3, in which the character of streamers array evolution is qualitatively different.

In regions 1 [i.e., at $R > R_t(E_0)$] and 2 [i.e., at $R_0(E_0) < R < R_c(E_0)$] expansion of streamers with time stops, and their form and parameters (E_M , σ^- , u_f) stop changing, that is, the entire array of streamers becomes a stationary ionization wave, with more or less strongly curved (corrugated) front (see Fig. 1). For these regions the tendency for a decrease of parameters E_M , σ^- , u_f and the front curvature along together with R is common (see Fig. 4).

For a description of these waves it is convenient to use the dimensionless coordinate system $\hat{\mathbf{r}} = (\mathbf{r} - u_f x)/R$, moving with the front, and look for a solution in the form of

$$\begin{pmatrix} \sigma(t, \mathbf{r}) \\ \rho(t, \mathbf{r}) \\ \varphi(t, \mathbf{r}) \\ \mathbf{E}(t, \mathbf{r}) \end{pmatrix} = \begin{pmatrix} \hat{\sigma}(\hat{\mathbf{r}}) \\ (\tilde{\alpha}R)^{-1}\hat{\rho}(\hat{\mathbf{r}}) \\ \tilde{E}R\hat{\varphi}(\hat{\mathbf{r}}) \\ \tilde{E}\mathbf{F}(\hat{\mathbf{r}}) \end{pmatrix}. \quad (15)$$

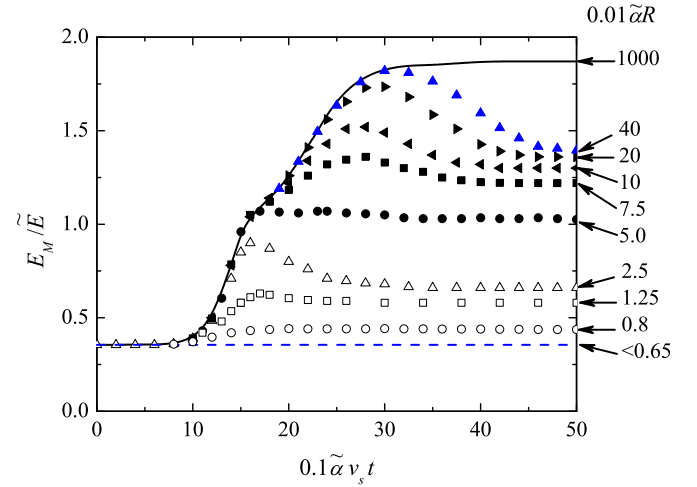


FIG. 2. (Color online) Maximum field strength E_M in the streamers array vs time at $E_0 = 0.36\tilde{E}$ and different values of R . Open symbols: calculation with $R_0 < R < R_c$; dark symbols: calculation with $R > R_t$; values for R_0, R_c, R_t are given in caption to Fig. 3. Solid line: calculation for an isolated streamer; dashed line: the external field E_0 .

The substitution of (15) into (5)–(7) leads to a system of equations

$$\frac{u_f}{R} \frac{\partial \hat{\sigma}}{\partial \hat{x}} + 2 \left(\hat{\sigma} v \alpha + \frac{q g_t}{\varepsilon \tilde{\alpha} \tilde{E}} \right) = \frac{1}{R^2} \left[\frac{1}{\tilde{\alpha}} \hat{\nabla} \cdot (\hat{\rho} \mathbf{v}) - \Delta \hat{\sigma} \right], \quad (16)$$

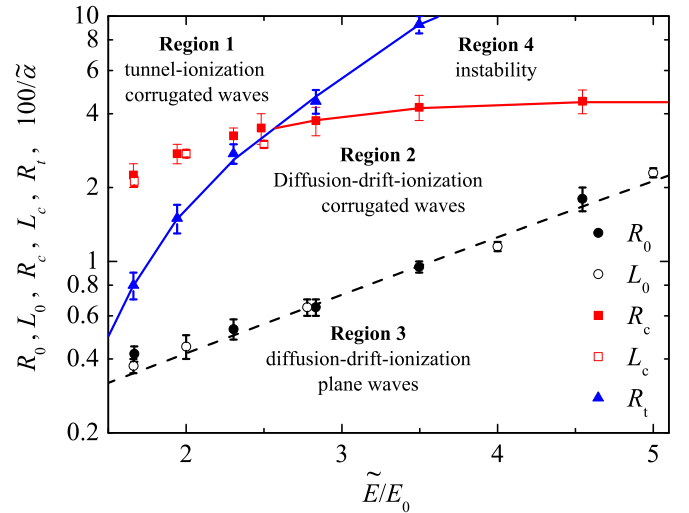


FIG. 3. (Color online) Diagram of steady states of the hexagonal streamers lattice. Lines separate the plane $[1/E_0, R]$ into four qualitatively different regions (see text). Triangles: at $R < R_t$ tunneling ionization is negligible. Solid squares: at $R > R_c$ the local transverse instability of the 3D front arises if tunneling ionization is negligible (with $E_0 > 0.4\tilde{E}$). Open squares: at $L > L_c$ the local transverse instability of the 2D front in gases arises (according to Ref. [8]). Circles: at $R < R_c$ (hexagonal 3D array, solid circles) and $L < L_c$ (2D array, open circles) perturbations generated by the primary avalanche decay. Dashed line: calculation from formulas (28) and (29).

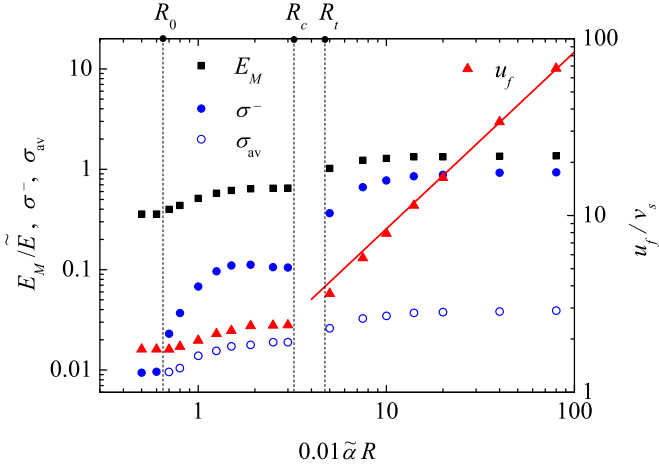


FIG. 4. (Color online) Maximum field strength E_M , front velocity u_f , maximum σ^- , and the average over the area σ_{av} concentrations of charge carriers behind the front vs parameter R at $E_0 = 0.36\tilde{E}$.

$$\frac{u_f}{R} \frac{\partial \hat{\rho}}{\partial \hat{x}} - \hat{\nabla} \cdot (\hat{\sigma} \mathbf{v}) = -\frac{D}{\tilde{\alpha} R^3} \hat{\Delta} \hat{\rho}, \quad (17)$$

$$\hat{\nabla} \cdot \mathbf{F} = \hat{\rho} = -\hat{\Delta} \hat{\phi}, \quad (18)$$

where differential operators $\hat{\nabla}$ and $\hat{\Delta}$ are with respect to $\hat{\mathbf{r}}$.

In region 1 the maximum field strength at the front E_M reaches a sufficiently large value (of the order of \tilde{E} with our chosen values of semiconductor parameters) for tunneling ionization to become noticeable. For very large R shape of the front $y_f(x)$ and parameters E_M , σ^- are independent on R , the space charge density $q\rho \propto 1/R$, and the velocity $u_f \propto R$, and much higher than the maximum drift velocity v_s (see Fig. 4). These scaling laws are a direct consequence of the structure equations (16)–(17): their right-hand sides are negligible at $R \rightarrow \infty$, and the dimensionless function $\hat{\sigma}(\hat{\mathbf{r}})$, $\hat{\rho}(\hat{\mathbf{r}})$, $\hat{\phi}(\hat{\mathbf{r}})$, and $\mathbf{F}(\hat{\mathbf{r}})$ cease to depend on R , if the front velocity $u_f \propto R$.

It is interesting to note that the solution (15) is quite similar to the exponentially self-similar solution (4) of Refs. [36,41], which describes evolution of a standalone streamer in a uniform field in infinite space. The only distinction is that exponentially growing spatial scale in our case does not depend on time and is equal to R . Therefore the rise time of the spatial scale, entering into the exponentially self-similar equations (11) and (12) of Refs. [36,41], is replaced by time, for which the front moves ahead for distance R in Eqs. (16) and (17) without their right-hand sides. The principle is that both types of self-similarity realize only for sufficiently large R and u_f , when the terms with the factors R^{-2} or u_f^{-2} can be neglected. The physical meaning of this approach lies in the fact that for large R the front velocity u_f is much more than the average directed velocity of the charge carriers. In this limit, their transport is not directly involved in the variation of σ , which is caused exclusively by the ionization as described by (16). The role of the drift is reduced to the formation of the space charge [see Eq. (17)], which suppresses the field behind the front according to Poisson equation (18), and determines the structure of a wave as a whole.

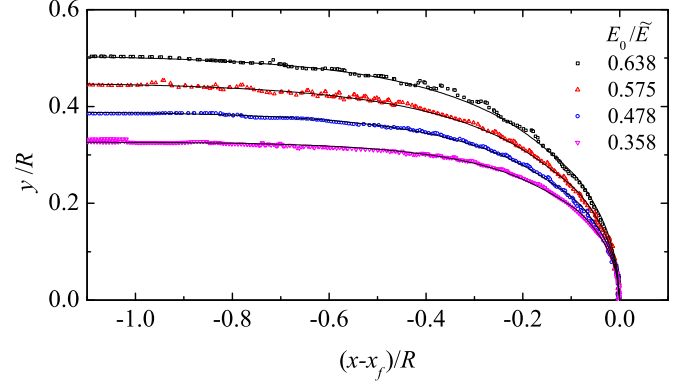


FIG. 5. (Color online) Steady-front shapes of a hexagonal lattice of streamers with $\tilde{\alpha}R = 8000$ and various external field strengths E_0 . The symbols indicate the positions of the points behind the front, where the field strength on the results of the numerical simulation is equal to $0.001\tilde{E}$. Lines: approximation by formula (1).

Dependencies $y_f(x)$ for such distant streamers shown in Fig. 5 are well described by a function (1) after replacement of L to R . However, for the reasons mentioned in the introduction, the function (1) should be considered only as one of the suitable approximations of the simulation results. Fitting parameters a, b included in it depend on E_0 essentially (see Fig. 6), moreover $a \neq b$ and $(a + b) \neq 1$. Dependencies of other front parameters on E_0 are shown for this case in Figs. 7–9.

As expected, the maximum field strength at the front E_M increases with E_0 at small E_0 (Fig. 7); along with E_M dimensionless time $u_f / \tilde{\alpha} R v_s$ for which the front moves ahead at distance R (Fig. 7) and the concentration of σ^-, σ_{av} (Fig. 8), all of which are independent on R , increase too. However, the ratio E_M / E_0 decreases (see Fig. 9). To explain this effects, it should be noted that with increasing $(x_f - x)$ field E_n and hence ionization rate $v_s \alpha(E)$ decreases rapidly and becomes negligible at $x < x_i$, where $E_n < E_i \equiv E_n(x_i) \sim 0.1\tilde{E}$. It is clear that the length $(x_f - x_i)$ of the ionization region increases with E_M and E_0 , so radius bR of each streamer in the array

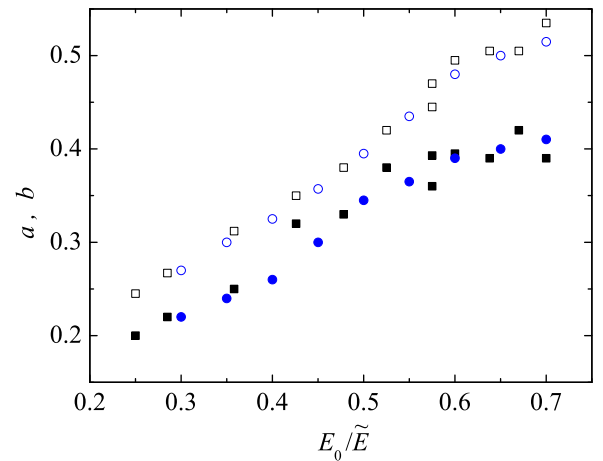


FIG. 6. (Color online) The parameters a (filled symbols) and b (open symbols), which determine the steady-front shapes of the streamers array [see (1)] vs the external field strength E_0 with $\tilde{\alpha}R = 8000$ (squares) and $\tilde{\alpha}R = 4000$ (circles).

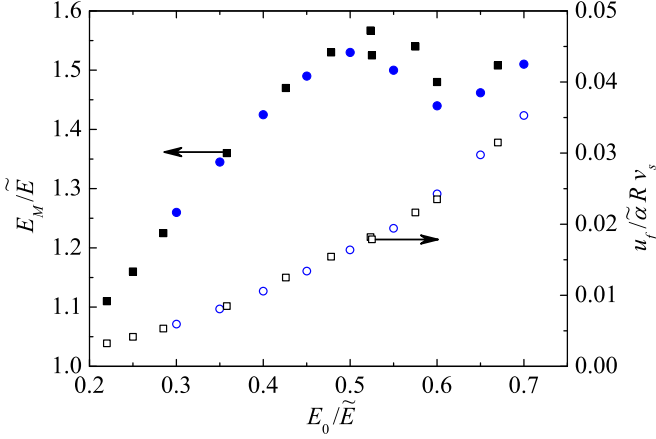


FIG. 7. (Color online) Maximum field strength E_M and dimensionless time of flight $u_f/\tilde{\alpha}Rv_s$ of the front distance R vs the external field strength E_0 with $\tilde{\alpha}R = 8000$ (squares) and $\tilde{\alpha}R = 4000$ (circles).

must also increase. The parameter a , characterizing the degree of “sharpness” of a streamer front,² also increases with E_0 , but more slowly than b . In other words, this means that streamers have to become sharper, but thicker when E_0 rises (Fig. 5). The results of numerical calculations of E_M for the simplest model of the streamers (see the Appendix) show that the combined effect of these two factors should lead to falling dependence E_M/E_0 on E_0 , which is consistent with the simulation results (see Fig. 9) in qualitative terms. Some excess of the expected relations over observable E_M/E_0 is due to the fact that the front of the streamer has a finite thickness δ , and the ratio of δ/R increases with E_0 [37]. The function $E_M(E_0)$ (and, hence, function $\sigma^-[E_M(E_0)]$, which does not depend on the front shape [11]) saturates at large E_0 (Figs. 7, 8). At the same time the front velocity u_f increases not only with growth of E_M , but also with the recession slowing the field strength ahead of the front [36,37]. Therefore, the function $u_f(E_0)$ is not saturated even at the highest E_0 (Fig. 7).

Here we must mention an important result for practical applications: the average concentration σ_{av} of electrons and holes behind a corrugated ionization wave is much more than behind the front of a plane wave (Fig. 8). The reason for this is that the reduction of the ionization area b^2 times in a corrugated wave compared with a flat one is compensated by an exponential increase of impact ionization rate. This effect is particularly large in a relatively weak external field, where the dependence of $\alpha(E)$ is very sharp.

With decreasing R it becomes apparent that the front resembles not a cylinder with an oval tip, but a badminton shuttlecock (Fig. 1), and the slope of almost linear section of $y_f(x)$ (shuttlecock feathers) decreases approximately inversely proportional to R (Fig. 10), and approximation (1) is becoming less suitable for small R . To explain this effect, it should be noted that in the case of a stationary wave the

²The more a , so the streamer front is sharper at a fixed value bR because the curvature of line $y_f(x)$ is equal to a/b on the x axis.

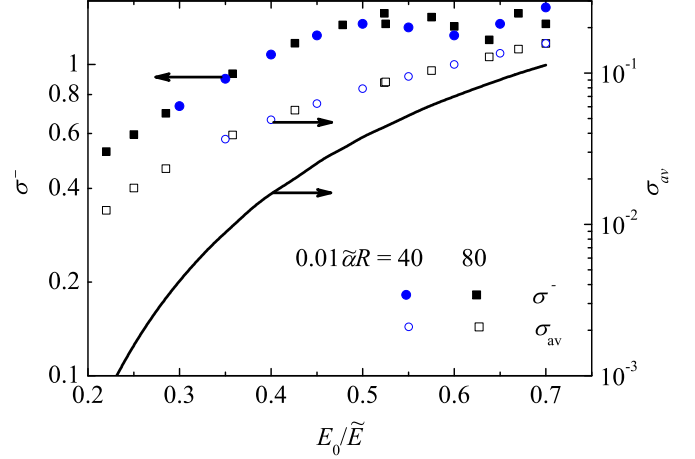


FIG. 8. (Color online) Maximum σ^- and the average over the area σ_{av} concentrations of charge carriers behind the front vs the external field strength E_0 with $\tilde{\alpha}R = 8000$ (squares) and $\tilde{\alpha}R = 4000$ (circles). Line: calculation of σ^- for a plane wave.

kinematic relation

$$\frac{dy_f}{dx} = -\frac{u_n}{\sqrt{u_f^2 - u_n^2}} \quad (19)$$

holds, where $u_n = u_n[E_n(x)]$ ³ and $y_f(x_f) = 0$, $u_n(x_f) = u_f$ by definition. In the area of $x < x_i$ the front itself ceases to be an ionization front, and it is just a thin layer of a space charge, moving mainly due to an electron (if $\rho < 0$ at the front) or holes (if $\rho > 0$ at the front) drift, so $u_n = v[E_n(x)]$. From this and the scaling laws $u_f \propto R$, $E_M = \tilde{E}F(0,0)$, it follows that the derivative of dy_f/dx tends to zero, and the streamers radius tends to a constant value of bR at $R \rightarrow \infty$ and $u_f/v_s \rightarrow \infty$. It is easy to show that in this case the field E_n behind the front decreases like

$$E_n(x) \approx E_i \exp[\lambda_E(x - x_i)], \quad (20)$$

where

$$\lambda_E \approx \frac{1}{R} \left(\frac{1.85}{1-b} - 1 \right) \quad (21)$$

is a minimal positive root of the equation

$$J_0(\lambda_E b R) Y_1(\lambda_E R) = J_1(\lambda_E R) Y_0(\lambda_E b R); \quad (22)$$

J_ν and Y_ν are Bessel functions of the first and second kind of order ν . The substitution of (20) in (19) leads after integration to asymptotic dependence

$$y_f(x) = bR - \frac{v}{\lambda_E \sqrt{u_f^2 - v^2}} \ln \left[1 + \frac{E_i}{E_s} e^{\lambda_E(x-x_i)} \right], \quad (23)$$

³The kinematic condition (19) of front stationarity is usually written in the equivalent form $u_n = u_f \cos \vartheta$, where ϑ is the angle between the front normal and the x axis (see, e.g., Refs. [39,40]). If the wave propagation is significantly affected by tunnel ionization, velocity u_n depends not only on E_n , but also on the whole field distribution along a force line intersecting the front [36,37]. This makes the analytical calculation of the whole front form quite so hopeless, but has no effect on the properties of the function $y_f(x)$ at $x < x_i$.

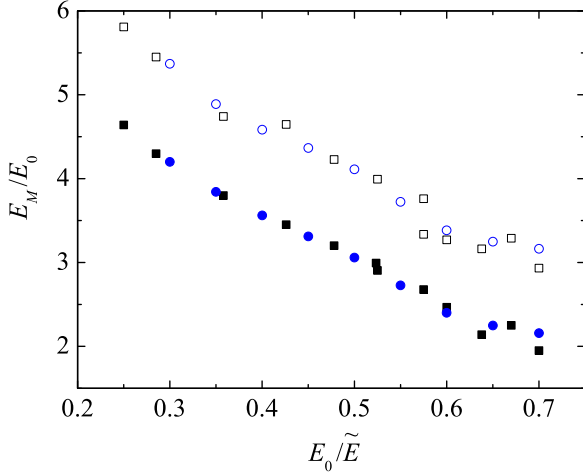


FIG. 9. (Color online) Ratio E_M/E_0 vs the external field strength E_0 with $\tilde{\alpha}R = 8000$ (squares) $\tilde{\alpha}R = 4000$ (circles). Filled symbols: the simulation results, open symbols: calculation formulas (A1) using the values of a and b , shown in Fig. 6.

which is valid under the condition that the second term is small in comparison with the first term. In semiconductors, it is usually $E_i \gg E_s$, so there is an area where $E_s \ll E_n \leq E_i$, $v \approx v_s$ and

$$y_f(x) \approx y_f(x_i) - \frac{v_s}{\sqrt{u_f^2 - v_s^2}}(x - x_i) \quad (24)$$

according to the simulation results (see Figs. 1 and 10). The formula (24) should also be straight from (19) and therefore, in contrast to (23), is valid even if the ratio of u_f/v_s is not very

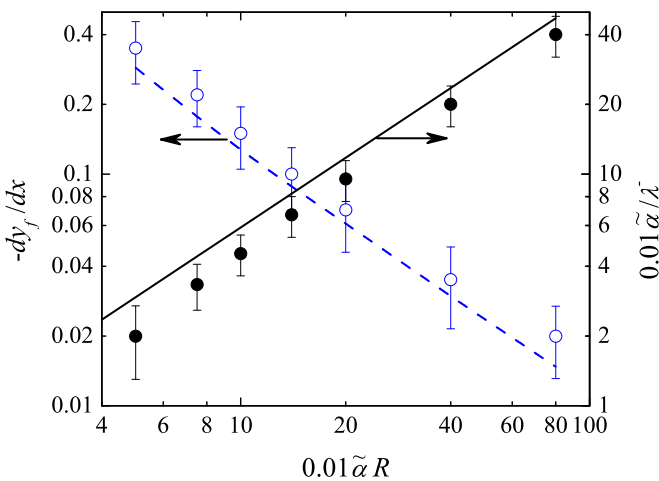


FIG. 10. (Color online) The derivative of dy_f/dx in the region of linearity of function $y_f(x)$ (open symbols) and the decay length $1/\lambda^{-}$ of the field behind the front (filled symbols) vs R with $E_0 = 0.36\tilde{E}$. Symbols are obtained by processing the simulation results, dashed line: calculation formulas (24) using the values of u_f , shown in Fig. 4, solid line: calculation formulas (21) using the values of b , shown in Fig. 6.

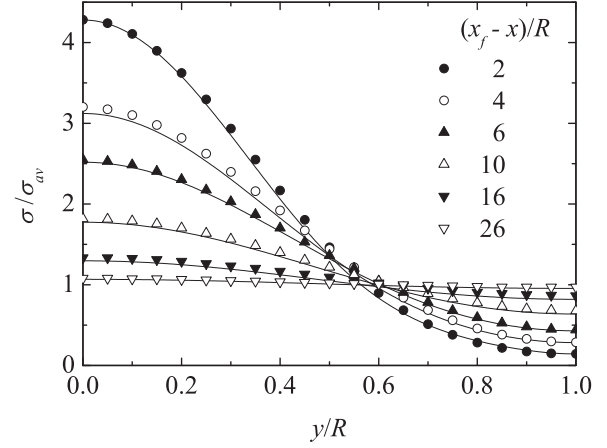


FIG. 11. The radial distribution of the charge carriers density σ at different distances from the front with $R = 100\tilde{\alpha}$ and $E_0 = 0.36\tilde{E}$. Line: the simulation results, symbols: the calculation formulas (27) with $\sigma_{av} = 0.0138$, $\sigma_{00} = 0.059$, and $\sigma_{0R} = 0.002$.

large.⁴ Consequently it is advisable to use an approximation

$$y_f(x) = \frac{2}{\pi} b_\infty R \arccos \left[\exp \left(\frac{\pi}{2} \frac{x - x_f}{aR} \right) \right] - \frac{v_s}{\sqrt{u_f^2 - v_s^2}}(x - x_f), \quad (25)$$

which is consistent with (24) in the region $(x_f - x) > 2aR$ at an appropriate choice of b_∞ , coincides with (1) at $v_s/u_f \rightarrow 0$ and well describes the shape of the front at all ratio v_s/u_f as long as $E_n > E_s$.

At more higher values of $(x_f - x)$ the inequality $E_n \ll E_s$ is satisfied, so it follows from (23), that function $y_f(x)$ seeks to bR exponentially:

$$y_f(x) = bR - \frac{\mu_0 E_i}{\lambda E u_f} e^{\lambda E (x - x_i)}, \quad (26)$$

where $\mu_0 = v_s/E_s$ is low-field mobility. In gases $E_s \gg E_i$ (that is, $\mu = \mu_0$ in the topical range of fields); therefore the range of linearity of $y_f(x)$ has to be absent, which is consistent with the results of Ref. [8]. In a planar case $\lambda_E = \pi/2L(1 - b)$, so that formula (26) correctly describes the asymptotic of function (1) at $(x_f - x) \rightarrow \infty$, obtained as a result of an exact solution of the corresponding problem. This coincidence confirms the correctness of the above approximate method for determining the shape of the front at $x < x_i$.

However, it must be borne in mind that due to the exponential decrease of the field strength E_n and the corresponding front surface charge density the front as such actually ceases to exist just where formula (26) is formally applicable for semiconductors. Instead, the filament of quasineutral plasma arises and fills the entire area of $y < R$, but this filament is highly nonuniform in the transverse direction. The main transport mechanism of the electrons and holes are becoming

⁴It is interesting to note a precise analogy between this ionization front and the shock waves produced by supersonic motion of bodies in gases.

ambipolar diffusion, which results in a radial spreading of plasma, so that $\sigma \rightarrow \sigma_{av}$ at $x \rightarrow -\infty$ (Fig. 11). This process is well described by the formula

$$\begin{aligned} \sigma(x, y) &= \sigma_{av} + B \exp\left(\frac{x_0 - x}{x_1}\right) J_0\left(a_{11} \frac{y}{R}\right) \\ &\quad + C \exp\left(\frac{x_0 - x}{x_2}\right) J_0\left(a_{12} \frac{y}{R}\right), \\ B &= \frac{(\sigma_{00} - \sigma_{av})J_0(a_{12}) - \sigma_{0R} + \sigma_{av}}{J_0(a_{12}) - J_0(a_{11})}, \\ C &= \frac{(\sigma_{00} - \sigma_{av})J_0(a_{11}) - \sigma_{0R} + \sigma_{av}}{J_0(a_{11}) - J_0(a_{12})}, \end{aligned} \quad (27)$$

where $x_k = u_f R^2 / D a_{1k}^2$ and $a_{11} \approx 3.83$, $a_{12} \approx 7.02$ are the first and second roots of equation $J_1(x) = 0$, σ_{00} , and σ_{0R} is concentration in a plane $x = x_0 < x_i$ at $y = 0$ and $y = R$, respectively, which, like the σ_{av} , are determined by processing the simulation results. The formula (27) is obtained using the first two terms of the series (8.3) from Chapter VII of Ref. [42] and is applicable provided that $x_1 \gg D/u_f$, when the longitudinal diffusion is negligible. Formula (27) also helps to explain the fact that the transverse spreading of plasma is almost imperceptible in region 1, but it becomes a determinant at small $x_k \propto u_f R^2$, that is, in region 2.

In addition, the reduction of R also leads to two effects. First, E_M decreases so that when $R < R_t(E_0)$ a tunnel ionization ceases to have significant influence on the evolution of the streamers array, and at a relatively weak external field (at $E_0 < 0.4\tilde{E}$ in our case) the stationary distribution of streamers becomes impossible due to front transverse instability of each of them. Second, an even greater reduction of R suppresses the instability at last, and at $R < R_c(E_0)$ (in region 2 in Fig. 3) evolution of a streamers array again completes by the appearance of a stationary corrugated wave, which is propagating now not only due to drift and impact ionization, but also due to diffusion. The same mechanism determines the evolution of isolated streamers during a “diffusion stage” [11]. It is not surprising that the streamer front instability comes (according to Ref. [11]) where its radius is of the order of R_c . It is interesting to note that the front of two-dimensional streamers array in gases also becomes unstable [8], when distance $2L$ between them is more than $2R_c$ (see Fig. 3). The boundaries of the instability region (region 4 in Fig. 3) are also determined by the inequalities $R_t(E_0) > R > R_c(E_0)$, so it exists only at $E_0 < 0.4\tilde{E}$. In strong external fields tunneling ionization does not “turn off” and suppresses the instability even at $R < R_c(E_0)$.

With further decrease of R curvature of a corrugated front and parameters E_M , σ^- are also reduced. Primary avalanches begin to overlap before the avalanche-to-streamer transition and form a periodically perturbed stationary ionization front. The most long-wave harmonic of this perturbation is given by the boundary conditions of our problem and has a wave number $k = \pi/R$. Perturbation amplitudes (in particular, the difference $E_M - E_0$) decrease monotonically with R as long as become vanished at $R = R_0(E_0)$. At still lower R (in region 3) perturbations generated by the primary avalanche decay, so that over time a plane impact ionization wave arises. This result is consistent with the conclusions of a linear theory of

transverse instability of the impact ionization waves. For gases, such a theory was created by the authors of Ref. [15], which showed that the perturbations with $k < k_0 \approx \lambda^*/4$ had to increase with time, and the more short wave perturbations had to decrease. This approval is also true for semiconductor [17] if you use the appropriate to our case formula [30,31]

$$\lambda^* = \alpha_0 \sqrt{\frac{v_s}{D\alpha_0} - \frac{1}{2} + \sqrt{\frac{1}{4} + \frac{v_s}{D\alpha_0}}}, \quad (28)$$

where $\alpha_0 = \alpha(E_0)$. This means that at

$$R < R_0 \approx 4\pi/\lambda^* \quad (29)$$

an array of avalanches should produce a plane impact ionization wave⁵ in accordance with the results of modeling. This wave propagates with the same rate

$$u^* = \frac{D}{2} \left(3 + \sqrt{1 + \frac{4v_s}{D\alpha_0}} \right) \lambda^*, \quad (30)$$

for all $R < R_0$ [30,31] only due to drift, diffusion, and impact ionization, as the field strength at its front does not exceed E_0 and is insufficient for tunneling ionization. The formula (29) describes well the dependence of the critical radius R_0 (and coinciding with it the critical width L_0 for an array of flat streamers) on E_0 , obtained from the simulation (see Fig. 3).

Another feature of the corrugated ionization waves was found, but not explained, in Ref. [8]. It consists in the fact that the field behind the front tends to zero (in contrast to the isolated streamers [11,36]), but decays much more slowly than in the front of the plane waves. A typical example of such differences is presented in Fig. 12. The paradox of this effect is the following. In the case of stationary plane ionization waves, as it is easy to show, the field strength is attenuated by the law $\exp(\lambda^- x)$ with⁶

$$\lambda^- = \frac{u_f}{2D} \left(\sqrt{1 + 4\sigma^- v_s \frac{\tilde{\alpha} \tilde{E} D}{E_s u_f^2}} - 1 \right) \quad (31)$$

in exact agreement with the simulation results (see Fig. 12). The calculation of this formula for a corrugated wave always gives a significantly (almost four times in the case corresponding to Fig. 12) larger value of λ^- , but the simulation results give a significantly (approximately ten times) smaller value of λ^- .

The reason for this discrepancy is a curvature of the front. In a stationary wave conduction current is accurately compensated by displacement current, so that the total current density is zero everywhere.⁷ The situation is completely

⁵A similar effect was observed earlier in the simulation of flame propagation in a tube [43]: reduction of its diameter to a critical value corresponding to this process suppressed transverse instability, and the flame front remains flat.

⁶This formula is a bipolar analog of the formula (5.63) of Ref. [25].

⁷If the field ahead of the front of a stationary plane wave is not uniform (as in the $p^+ - n - n^+$ junction), then the total current density is not zero, but is constant everywhere [44], and the field strength behind the front approaching a finite value exponentially with exponent λ^- is also determined by formula (31).

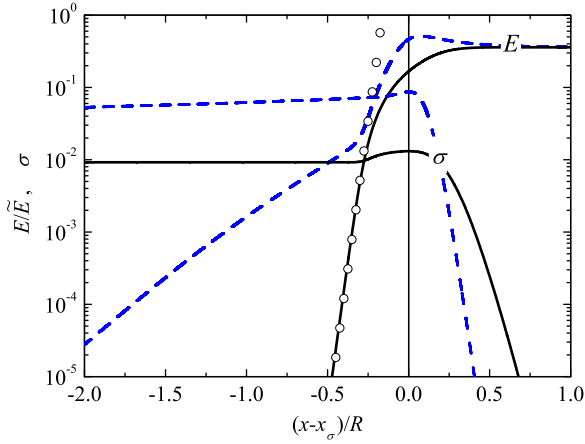


FIG. 12. (Color online) Distributions of the field strength E and charge carriers concentration σ along the x axis near the fronts of the plane (solid lines) and corrugated (dashed lines) waves with $R = 100\bar{\alpha}$ and $E_0 = 0.36\bar{E}$. Symbols: the calculation formulas (31) using the values of σ^- and u_f , obtained in the simulation of a plane wave. Concentration σ on the axis of x is maximal at $x = x_\sigma \lesssim x_f$.

different in corrugated waves. Near the x axis ahead of the front conduction current and the displacement current coincide with the direction of wave propagation, but the displacement current is opposite directed and dominates near the surface $y = R$ (where the concentration σ is very small). As a result, a vortex is shown in Fig. 13. Near the surface $y = R$ field strength, and with it the displacement current decay exponentially according to (20) with exponent λ_E . Obviously, the conduction current, providing the appearance of an ohmic field behind the front, decreases in the same way near the axis of x . It is clear that this ohmic field should decrease approximately exponentially with the increment of $\lambda_- \sim \lambda_E$. This conclusion is confirmed by the simulation results given in Fig. 10.

In conclusion of this section we will note two more circumstances. First, at given E_0 and R a stationary corrugated ionization wave is an attractor for a wide range of initial conditions; after sufficient time the same solution is

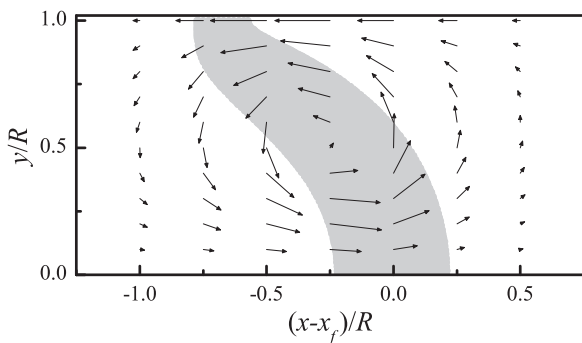


FIG. 13. The vector field of the current near the front of corrugated ionization wave at $R = 100\bar{\alpha}$ and $E_0 = 0.36\bar{E}$. Length of the arrows is proportional to yJ , where \mathbf{J} is the sum of the conduction and displacement current densities. The space charge density is more than $0.002\epsilon_0\bar{E} \approx 3.2 \text{ mC/cm}^3$ inside the region shaded in gray.

obtained:

- (1) For a point initial perturbation
- (2) For an ellipsoidal initial perturbation with a transverse semiaxis of order of $R/2$ (a similar result was obtained for the two-dimensional streamers array in gases [8])
- (3) As a result of restructuring a stationary corrugated wave with control parameters $\{F'_0, R\}$ after changing F'_0 to F_0
- (4) As a result of growth of small transverse perturbations of the plane ionization front, if $R < \pi/k_M$, where k_M is a wave number of the most rapidly growing perturbations [17] (similar scenarios of evolution are also realized during the propagation of plane fronts in various media, in particular, ionization fronts in gases [14], premixed flames [43,45], electrochemical doping fronts in organic semiconductors [46], etc.)

Second, apart from the above basic principles of evolution of interacting streamers, more subtle effects were found. In particular, at some values of control parameters E_0 and R , small quasiperiodic variations of the quantities σ behind the front and the maximum field strength E_M are observed, as well as small quasiperiodic deviations of the front shape from the linear function (24). A possible reason for such anomalies is the use of a too coarse finite element mesh, the minimum size of which is determined by the resources of our computers. However, we can not exclude the physical reality of the observed effects (see, for example, Ref. [25]).

IV. CONCLUSION

In the present article the results of numerical modeling of the evolution of the two-dimensional periodic array of identical streamers in a constant and uniform field are stated. It turned out that the nature of the evolution of a streamers array in semiconductors was much more complex in comparison with gases in a framework of “minimal model” [8]. The evolution of the array is completed in different ways, depending on the control parameters of the problem: the external field E_0 and the distance $2R$ between the streamers. For classification of various scenarios of evolution a diagram of the final state of the streamers array, dividing the plane of $[1/E_0, R]$ for four qualitatively various regions, is constructed and represented in Fig. 3. In regions 1 and 2 interaction between streamers leads over time to formation of two types of stationary ionization waves with the corrugated front, differing with ionization mechanisms. Specific characteristics of the fronts of these waves, caused by features of processes of ionization and charge transport in semiconductors, are described in detail and explained on the basis of simple physical reasons. In region 3, at enough small R , the array of primary avalanches generates a planar impact ionization wave. In weak external fields between regions 1 and 2 there is region 4 in which stationary propagation of ionization waves is impossible because of development of transverse instability. This instability observed earlier at modeling of isolated streamers can be called *local* because it destroys (or does not destroy) fronts of each streamer in the array.

However, besides it *global* instability of array of streamers (each of which is locally stable) is also possible. In fact, in this work we considered that the primary avalanches generating the array of streamers, started *at the same time* from nodes of a *ideal* planar hexagonal lattice. Meanwhile small deviations in

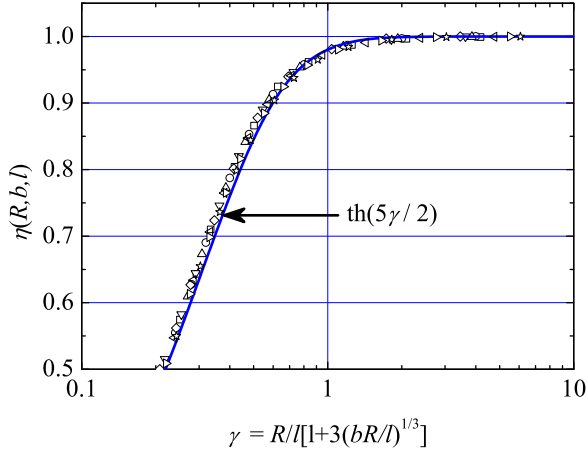


FIG. 14. (Color online) Ratio of the maximum field strength at a single cylinder and an array of cylinders with hemispherical caps $\eta(R, b, l)$ vs their length $2l$, radius bR , and distance between them $2R$ with $bR/l = 0.01\text{--}0.25$ and $R/l = 0.4\text{--}50$.

time and/or in the provision of avalanches starting will lead to emergence of “competition” between streamers of the nonideal array: some of them will appear in a “preferred position” and will develop quicker than others. Sooner or later such streamers will start reducing considerably a field strength in the vicinity and suppress propagation of neighbors. If distance d between the electrodes is sufficiently large, only the earliest and/or most remote from neighbors streamers will be able to overcome it, and the average distance between such leading streamers should be of the order of $3d$ (see the Appendix). These reasons indicate the importance of a global instability problem, which will be analyzed in a separate paper.

ACKNOWLEDGMENTS

The author is grateful to A. V. Gorbatyuk for helpful discussions. This work was supported by RFBR (Grant 13-08-00474).

APPENDIX: THE ELECTROSTATIC INTERACTION BETWEEN METAL CYLINDERS WITH ELLIPSOIDAL TIPS

For a quick estimate of a maximum field strength E_M of streamers in the array each of them can be represented in the form of a metal cylinder of length $2l$ with a radius bR and tips

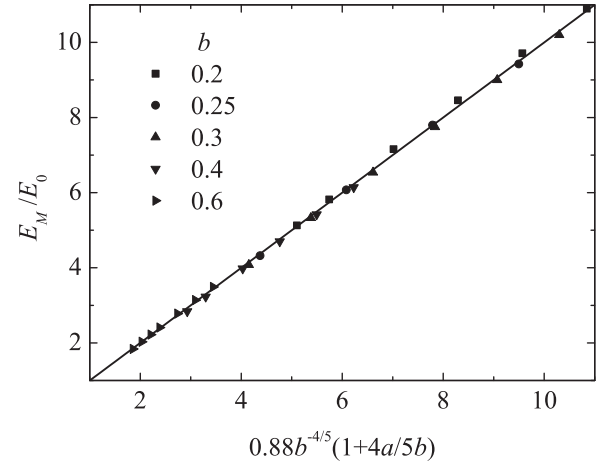


FIG. 15. Ratio E_M/E_0 for an array of cylinders with ellipsoidal tips vs the dimensionless length of the longitudinal $a_e = \pi a/2$ and transverse b semiaxes with $b = 0.2\text{--}0.6$ and $a_e = 0.2\text{--}1.2$.

in the form of ellipsoids of rotation. To interpret the simulation results you need to know how the array parameters affect the two values.

The first of these, the ratio of $\eta(R, b, l) \equiv E_M(R, b, l)/E_M(\infty, b, l)$, allows us to define the conditions under which the influence of the electrostatic interaction between streamers on E_M becomes noticeable. These conditions depend little on the longitudinal axis of the ellipsoids $a_e R$; therefore, when calculating η it would be possible to put $a_e = b$ for simplicity. The results of these calculations are shown in Fig. 14. As can be seen, for all relevant values of b and R/l they are well described by the function $\eta = \tanh(5\gamma/2)$, where $\gamma = R/l[1 + 3(bR/l)^{1/3}]$. Interaction becomes significant when η is noticeably different from the one that is at $\gamma \lesssim 1$ or $R \lesssim (2.5\text{--}3)l$.

The second desired value, the ratio $E_M(b, a_e)/E_0$ at $l \gg R$, allows us to evaluate E_M in a stationary propagating of streamer array (or, in other words, in a stationary corrugated ionization wave). In this case, the result depends strongly not only on b , but also on a_e . We used the value $a_e = \pi a/2$, since in this case the difference between the system “cylinder ellipsoid” and the surface of revolution with generating lines a kind of (1) is minimal and for all a, b does not exceed 5%. The results of such calculations, presented in Fig. 15, are well described by the dependence

$$E_M(a, b) = 0.88E_0b^{-4/5}(1 + 4a/5b). \quad (\text{A1})$$

[1] Yu. D. Korolev and G. A. Mesyats, *Physics of Pulsed Breakdown in Gases* (Nauka, Moscow, 1991) (in Russian).
 [2] E. M. Bazelyan and Yu. P. Raizer, *Spark Discharge* (CRC Press, Boca Raton, FL, 1998).
 [3] S. Nijdam1, F. M. J. H. van de Wetering, R. Blanc, E. M. van Veldhuizen, and U. Ebert, *J. Phys. D* **43**, 145204 (2010).
 [4] T. M. P. Briels, E. M. van Veldhuizen, and U. Ebert, *IEEE Trans. Plasma Sci.* **36**, 906 (2008).

[5] A. V. Krasnochub, E. I. Mintoussov, M. M. Nudnova *et al.*, Proc XXVIII ICPIG, Eindhoven, the Netherlands, 18–22 July, 2005, <http://www.icpig2005.nl>.
 [6] R. Ono and T. Oda, *Int. J. Plasma Environ. Sci. Tech.* **1**, 123 (2007).
 [7] G. V. Naidis, *J. Phys. D* **29**, 779 (1996).
 [8] A. Luque, F. Brau, and U. Ebert, *Phys. Rev. E* **78**, 016206 (2008).
 [9] U. Ebert, W. van Saarloos, and C. Caroli, *Phys. Rev. Lett.* **77**, 4178 (1996); *Phys. Rev. E* **55**, 1530 (1997).

- [10] F. Brau, A. Luque, B. Meulenbroek, U. Ebert, and L. Schafer, *Phys. Rev. E* **77**, 026219 (2008).
- [11] A. S. Kyuregyan, *JETP* **109**, 833 (2009).
- [12] M. Arrayas and U. Ebert, *Phys. Rev. E* **69**, 036214 (2004).
- [13] M. Arrayas, M. A. Fontelos, and J. L. Trueba, *Phys. Rev. Lett.* **95**, 165001 (2005).
- [14] M. Arrayas, S. Betelu, M. A. Fontelos, and J. L. Trueba, *SIAM J. Appl. Math.* **68**, 1122 (2008).
- [15] G. Derks, U. Ebert, and B. Meulenbroek, *J Nonlinear Sci.* **18**, 551 (2008).
- [16] M. Arrayas, M. A. Fontelos, and U. Kindelan, *Phys. Rev. E* **86**, 066407 (2012).
- [17] A. S. Kyuregyan, *Thermal Eng.* **58**, 1119 (2011).
- [18] P. G. Saffman and G. I. Taylor, *Proc. R. Soc. A* **245**, 312 (1958).
- [19] P. G. Saffman, *J. Fluid Mech.* **173**, 73 (1986).
- [20] D. Bensimon, L. P. Kadanoff, S. Liang, B. I. Shraiman, and C. Tang, *Rev. Modern Phys.* **58**, 977 (1986).
- [21] S. J. Chapman and J. King, *J. Eng. Math.* **46**, 1 (2003).
- [22] E. D. Lozansky and O. B. Firsov, *J. Phys. D* **6**, 976 (1973).
- [23] E. D. Lozanski and O. B. Firsov, *Spark Theory* (Atomizdat, Moscow, 1975) (in Russian).
- [24] M. Arrayas and M. A. Fontelos, *Phys. Rev. E* **84**, 026404 (2011).
- [25] A. N. Lagarkov and I. M. Rutkevich, *Ionization Waves in Electrical Breakdown in Gases* (Springer, New York, 1994).
- [26] S. N. Vainshtein, Yu. V. Zhilyaev, and M. E. Levinstein, *Pis'ma Zh. Tekh. Fiz.* **14**, 1526 (1988) [*Sov. Tech. Phys. Lett.* **14**, 664 (1989)].
- [27] A. S. Kyuregyan, *Tech. Phys. Lett.* **31**, 1043 (2005).
- [28] I. V. Grekhov, *Solid-State Electron.* **32**, 923 (1989).
- [29] R. J. Focia, E. Schamiloghu, C. B. Fledermann, F. J. Agee, and J. Gaudet, *IEEE Trans. Plasma Sci.* **25**, 138 (1997).
- [30] A. S. Kyuregyan, *JETP Lett.* **86**, 308 (2007).
- [31] A. S. Kyuregyan, *Semiconductors* **42**, 21 (2008).
- [32] P. Rodin, U. Ebert, W. Hundsdorfer, and I. Grekhov, *J. Appl. Phys.* **92**, 958 (2002).
- [33] P. Rodin and I. Grekhov, *Appl. Phys. Lett.* **86**, 243504 (2005).
- [34] P. Rodin, A. Rodina, and I. Grekhov, *J. Appl. Phys.* **98**, 094506 (2005).
- [35] I. Grekhov and P. Rodin, *Tech. Phys. Lett.* **37**, 849 (2011).
- [36] A. S. Kyuregyan, *JETP* **110**, 637 (2010).
- [37] A. S. Kyuregyan, *Semiconductors* **47**, 978 (2013).
- [38] C. Li, U. Ebert, W. J. M. Brok, and W. Hundsdorfer, *J. Phys. D* **41**, 032005 (2008).
- [39] B. I. Shraiman, *Phys. Rev. Lett.* **56**, 2028 (1986).
- [40] X. Xie and S. Tanveer, *Arch. Rational Mech. Anal.* **166**, 219 (2003).
- [41] A. S. Kyuregyan, *Phys. Rev. Lett.* **101**, 174505 (2008).
- [42] H. S. Carslaw and J. C. Jaeger, *Conduction of Heat in Solids* (Clarendon Press, Oxford, 1994).
- [43] V. V. Bychkov, S. M. Golberg, M. A. Liberman, and L. E. Eriksson, *Phys. Rev. E* **54**, 3713 (1996).
- [44] A. S. Kyuregyan, *Semiconductors* **41**, 737 (2007).
- [45] V. V. Bychkov and M. A. Liberman, *Phys. Rep.* **325**, 115 (2000).
- [46] V. Bychkov, O. Jukimenko, M. Modestov, and M. Marklund, *Phys. Rev. B* **85**, 245212 (2012).